

Topological properties and the dynamical crossover from mixed-valence to Kondo-lattice behavior in golden phase of SmS

Chang-Jong Kang,* Hong Chul Choi, Kyoo Kim, and B. I. Min[†]

Department of Physics, Pohang University of Science and Technology (POSTECH), Pohang, 790-784, Korea
(Dated: November 2, 2021)

We have investigated temperature-dependent behaviors of electronic structure and resistivity in a mixed-valent golden phase of SmS, based on the dynamical mean-field theory band structure calculations. Upon cooling, the coherent Sm 4*f* bands are formed to produce the hybridization-induced pseudogap near the Fermi level, and accordingly the topology of Fermi surface is changed to exhibit a Lifshitz-like transition. The surface states emerging in the bulk gap region are found to be not topologically protected states but just typical Rashba spin-polarized states, indicating that SmS is not a topological Kondo semimetal. From the analysis of anomalous resistivity behavior in SmS, we have identified universal energy scales, which characterize the Kondo/mixed-valent semimetallic systems.

PACS numbers: 71.27.+a, 71.18.+y, 75.30.Mb

Kondo and mixed-valent physics in strongly-correlated 4*f* electron systems have been subject of longstanding controversy. It includes various interesting phenomena such as *p*-wave superconductivity and non-Fermi-liquid behavior in heavy-fermion systems [1–3], and recently proposed topological Kondo insulator behavior in a typical mixed-valent insulator SmB₆ [3–6, 8–14]. The topological Kondo insulator of our present interest has attracted a great deal of recent attention. However, the realization of the topological properties in SmB₆ is still under debate. The immediate question was addressed whether a similar mixed-valent system, SmS, also has the topological properties or not. Indeed, the mixed-valent golden phase of SmS (g-SmS) was reported to be a topological Kondo semimetal [15].

SmS has been studied for last four decades [4, 5, 7, 16, 17, 19, 21, 22, 24–37], but there remain several issues still unresolved. SmS crystallizes in a face-centered cubic (fcc) structure of rock-salt (NaCl-type) type. At the ambient pressure, SmS has a so-called black phase, which is a semiconductor with indirect and direct band gaps of 90 meV and 0.4 eV, respectively [24]. In the black phase of SmS (b-SmS), the valence state of Sm is divalent (2+), and so the system is nonmagnetic. Under high pressure above 6.5 kbar, SmS undergoes a first-order isostructural phase transition from b-SmS to g-SmS, in which Sm ions are mixed-valent with the average valency of 2.6+ ~ 2.8+ [25, 26]. This isostructural transition is accompanied by the volume collapse as much as 15% [25], as shown in Fig. 1(b).

The energy gap decreases monotonically with increasing the pressure. It is controversial whether g-SmS has a real gap or a pseudo-gap [27, 28]. The resistivity behavior of g-SmS is quite anomalous in the sense that the overall behavior is Kondo-lattice like but it exhibits a couple of abnormal hump structures [33–37]. Applying the pressure further, g-SmS has a magnetic instability at about 19.5 kbar with the antiferromagnetic order [31–33].

Above 19.5 kbar, the resistivity shows a metallic behavior and the valence state of Sm increases toward 3+ [33].

There have been several reports on the density-functional theory (DFT)-based band structure study of SmS [15–17]. But even the ground-state insulating nature of b-SmS is not properly described by the DFT-based schemes, and so the advanced methods like the dynamical mean-field theory (DMFT) should be employed to investigate the topological properties in g-SmS that has the strongly-correlated 4*f* electrons. Here we have investigated electronic structures of SmS, based on the DMFT scheme. First, we have shown that the electronic properties of b-SmS are described properly only by the DMFT scheme. Then we have examined the *T*-dependent electronic structure evolution in g-SmS. Upon cooling, the 4*f* states form the coherent 4*f* bands with a pseudo-gap feature near the Fermi level (E_F), and accordingly the topology of the Fermi surface (FS) is changed, which is reflected well in the anomalous resistivity behavior in g-SmS. We have demonstrated that the surface states realized in g-SmS are not the topological

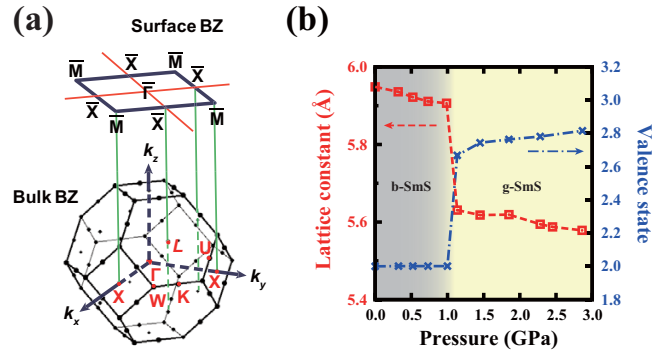


FIG. 1: (Color Online) Isostructural phase transition in SmS. (a) Bulk and surface Brillouin zones (BZs) of fcc SmS. (b) The pressure dependence of the lattice constant and the Sm valence state of SmS (Data taken from Ref. [22]).

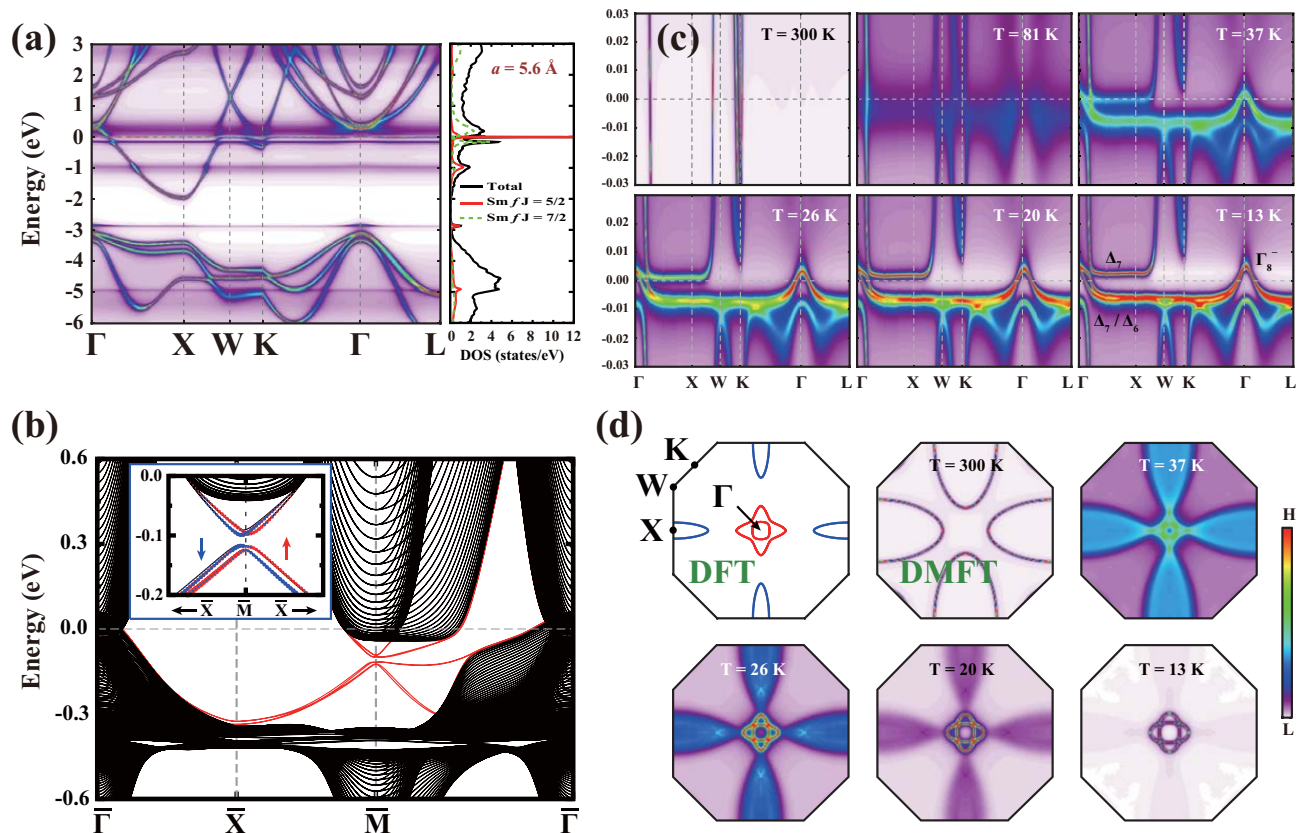


FIG. 2: (Color Online) Electronic structure of g -SmS ($a = 5.6 \text{ \AA}$). (a) The DMFT band structure at $T = 13 \text{ K}$. (b) Surface band structure obtained by the model slab calculation based on the DFT band structure. The surface states in the inset manifests a typical Rashba splitting with a tiny gap, and so they are not topologically protected states. (c) T -dependent band structures in the DMFT scheme. Upon cooling, the coherent Sm $4f$ band emerges near E_F , and the hybridization gap appears below $T = 26 \text{ K}$. (d) T -dependent FS evolution in the DMFT scheme, which is compared with the DFT FS with 10 times enhanced SOC of Sm $4f$ -electron (top-left) [39]. Upon cooling, X -centered d -band pockets are reduced, while f -band pockets emerge at Γ .

states, but are just the typical Rashba states.

We have employed the all-electron FLAPW band method implemented in Wien2k [1]. We have checked that both the DFT and the DFT+ U (on-site Coulomb U) schemes can not describe the ground state insulating electronic structure of SmS properly (see the supplement [39]). Therefore, we have employed the combined DFT and DMFT (DFT+DMFT) approach implemented in Wien2k, which has successfully reproduced many aspects of the strongly-correlated electron systems [40, 41]. We used projectors in the large window of 10 eV, and the on-site Coulomb and exchange energies of $U = 6.1 \text{ eV}$, $J = 0.8355 \text{ eV}$ were adopted to fit in X-ray photoemission spectroscopy (XPS) data (see Fig. S2 for the DMFT band structure of b -SmS in the supplement) [7]. To solve the impurity problem, the non-crossing approximation (NCA) is used [8, 13]. To verify the justification of the NCA scheme, we have also used the continuous time quantum Monte Carlo scheme for b -SmS and checked that two schemes give the same result.

The DMFT band structure and DOS of g -SmS ($a =$

5.6 \AA) at $T = 13 \text{ K}$ are shown in Fig. 2(a). Notable is the flat Sm $4f$ bands near E_F , which yield sharp Kondo resonance-like peaks in the DOS (see Fig. 3(a)). The $4f$ -band in the vicinity of E_F is mainly of $J = 5/2$ character ($4f_{5/2}$), while $4f_{7/2}$ bands are located at about $\pm 0.17 \text{ eV}$ from E_F . These coherent Sm $4f$ bands hybridize strongly with Sm $5d$ band to produce the hybridization gap near E_F (see Fig. 2(c)). However, the $4f_{5/2}$ (Γ_8^-) band at Γ is above E_F , and so the band structure exhibits the metallic nature having the mixed-valent state of $\text{Sm}^{2.73+}$. The Γ_8^- band is dispersive with the band width of about 0.03 eV, as in SmB₆ [3]. The DMFT band structure near E_F is analogous to the band structure obtained by the DFT+SOC (SOC: spin-orbit coupling), as shown in the supplement [39], but the band width of the former is nearly ten times smaller than that of the latter, which is also similar to the case in SmB₆ [3, 8].

Even though g -SmS has metallic nature, the band inversion occurs at X , and so it is tempting to anticipate the topologically protected surface states in SmS [15]. To check the topological property, we have examined the

surface band structure in Fig. 2(b), which was obtained by the model slab calculation based on the DFT bulk band structure [42]. The surface states, however, have a tiny gap instead of a Dirac cone and the momentum-dependent splitting of spin states, which reveals that they are not topologically protected states but just Rashba spin-polarized surface states. This result is a contrast to that of Li *et al.* [15], who argued that g-SmS is to be a topological semimetal. The charge gap protection is essential to have the topological nature. In this respect, La-doped SmS can be a better candidate for a topological Kondo insulator, because $\text{Sm}_{0.75}\text{La}_{0.25}\text{S}$ under pressure was reported to be an excitonic insulator with an energy gap of 1 meV [43].

Figure 2(c) shows the T -dependent band structures of g-SmS ($a = 5.6 \text{ \AA}$). At $T = 300 \text{ K}$, only the Sm d -band is seen to cut E_F . Upon cooling, Sm $4f$ spectra start to emerge near E_F at $T \simeq 80 \text{ K}$, and $4f_{5/2}$ bands are observed to be formed below $T \simeq 40 \text{ K}$. At $T = 26 \text{ K}$, the $4f_{5/2}$ hole bands near Γ (Γ_8^- quartet) forms the coherent band, and the hybridization gap between Sm $5d$ (t_{2g}) and $4f_{5/2}$ (Δ_7) bands begins to appear at the crossing point near Γ . The coherence temperature T_{coh} is usually defined in metallic Kondo lattices as an onset T , at which the hybridization gap appears [44]. Note that T_{coh} is equivalent to T^* that is introduced in the two-fluid model for the Kondo lattice [45]. Hence $T = 26 \text{ K}$ is considered to be T_{coh} of g-SmS. In the Kondo lattice systems, T_{coh} can often be identified from the peak position of the resistivity, as will be discussed in Fig. 3(c). With decreasing T further, the separation between the upper $4f_{5/2}$ flat band (Δ_7 doublet) along $\Gamma - X$ and the lower $4f_{5/2}$ flat band (Δ_7/Δ_6 quartet) becomes enhanced, and eventually the former is shifted up above E_F at $T = 20 \text{ K}$. Below $T \simeq 13 \text{ K}$, it is seen that the $4f_{5/2}$ band becomes completely coherent over the whole Brillouin zone. In this case, the Γ_8^- hole band is still above E_F , and so SmS at very low T would exhibit metallic nature (see Fig. 3(c)).

Figure 2(d) presents the T -dependent FS evolution in g-SmS. Also presented is the DFT-FS, for comparison, which has X -centered electron ellipses and Γ -centered hole pockets. At $T = 300 \text{ K}$, the DMFT-FS arises solely from d -band, which produces the X -centered ellipses. Upon cooling, the ellipses become reduced more and more, and so almost disappear at $T = 13 \text{ K}$. Their spectral weights, however, become enhanced due to the contribution from the hybridized $4f_{5/2}$ band so as to have maximum intensity at $T \simeq 37 \text{ K}$. On the other hand, Γ -centered hole pockets originating from $4f_{5/2}$ (Γ_8^-) band begin to appear at $T \simeq 37 \text{ K}$, and are clearly manifested below $T_{coh} = 26 \text{ K}$. Therefore, the topology of the FS is to be changed twice, at $T \simeq 37 \text{ K}$ and $T \simeq 13 \text{ K}$. The former is due to the emergence of the coherent $4f$ band formation at Γ , while the latter is due to the separation of the upper $4f_{5/2}$ flat band (Δ_7 doublet) from E_F .

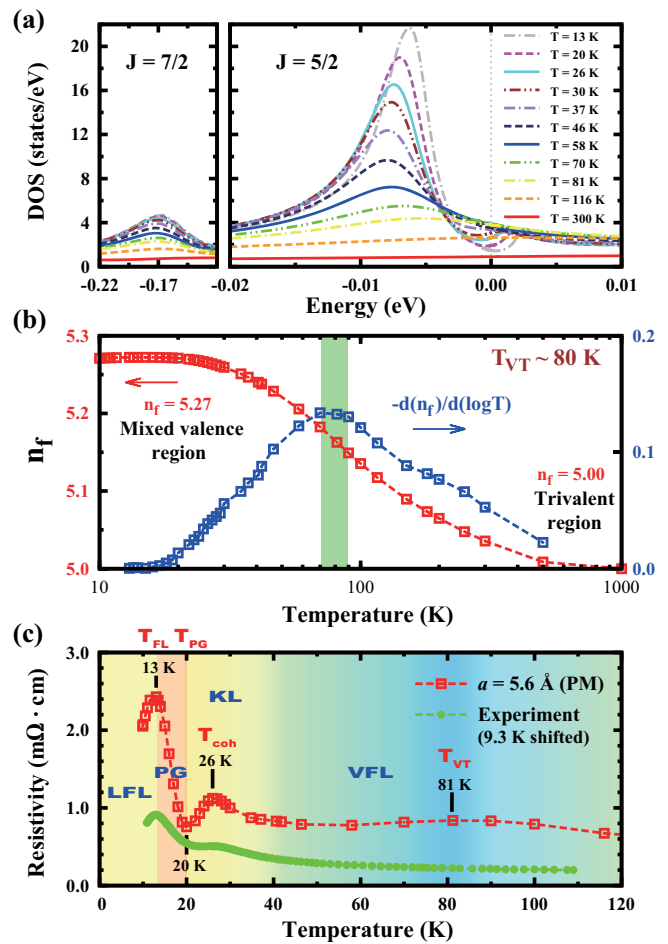


FIG. 3: (Color Online) T -dependent behaviors in g-SmS ($a = 5.6 \text{ \AA}$). (a) T -dependent DOS variation in the DMFT scheme. Upon cooling, the $J = 5/2$ DOS behaves like a Kondo resonance with the pseudo-gap like dip feature near E_F . The $J = 7/2$ DOS peak near -0.17 eV is also shown. (b) The number of occupied f -electrons (n_f) as a function of the logarithmic T scale. Upon cooling, n_f increases monotonically from trivalent state to the mixed-valent state. The effective valence-transition (VT) occurs at $T \simeq 80 \text{ K}$, as indicated by the peak in $-d(n_f)/d(\log T)$. (c) Resistivity vs. T obtained by the DMFT scheme. The experimental data are taken from Ref. [37], which are shifted by 9.3 K toward higher T . Upon cooling, SmS undergoes several crossover transitions from valence-fluctuation liquid (VFL), Kondo-liquid (KL), pseudogap (PG), to Landau Fermi-liquid (LFL).

This behavior is reminiscent of the Lifshitz transition that is a typical continuous quantum phase transition characterized by the topological change of the FS [46]. The feature in SmS is quite interesting because a Lifshitz-like transition occurs with the variation of T . Such a Lifshitz-like transition in g-SmS could be explored by ARPES and de Hass-van Alphen experiments. The change of the FS topology is well reflected in the T -dependent resistivity behavior in Fig. 3(c).

Upon cooling, the $4f_{5/2}$ DOS peak at $\sim -6 \text{ meV}$ be-

comes sharper and sharper, as shown in Fig. 3(a), resembling the T -dependent evolution of Kondo resonance. Noteworthy is the pseudo-gap feature near E_F , which arises from the f - d band hybridization below $T \simeq 30$ K, which is close to $T_{coh} = 26$ K. It is also seen that, upon cooling, the DOS at E_F increases first and then decreases below $T \simeq 80$ K [39]. The $4f_{7/2}$ DOS near -0.17 eV, which corresponds to the spin-orbit split side-band, behaves similarly to the $4f_{5/2}$ DOS upon cooling.

The number of f -electrons (n_f) in g-SmS versus T is presented in Fig. 3(b). Upon cooling, n_f increases monotonically from $n_f = 5$ (trivalent state) at high T to $n_f = 5.27$ (mixed-valence state) at low T . The increasing trend of n_f upon cooling has also been observed in SmB₆ [13, 47]. It is worthwhile to observe that n_f curve has an inflection point at $T \simeq 80$ K, which indicates that the effective valence-transition (VT) occurs at $T \simeq 80$ K.

Figure 3(c) shows the resistivity versus T of g-SmS evaluated in the DMFT scheme [44]. The overall behavior is that the resistivity increases upon cooling, but decreases below $T = 13$ K, as in metallic Kondo lattice systems. However, the detailed T -dependent behavior is quite anomalous. The calculated resistivity has a broad maximum at $T \simeq 80$ K, and starts to increase again at $T \simeq 40$ K to produce hump and dip structure at $T \simeq 26$ K and $T \simeq 20$ K, respectively. Upon further cooling, it exhibits another maximum at $T = 13$ K. Quite similar behavior is indeed observed in the measured resistivity of g-SmS [34–37], as shown in Fig. 3(c), even though the feature at $T \simeq 80$ K is not so obvious.

The anomalous behavior of the resistivity is closely correlated with the T -dependent evolution of electronic structure in Fig. 2(c)-(d). Namely, the broad maximum at $T \simeq 80$ K is considered to arise from the dynamical valence-fluctuation (VF), as manifested by the effective VT in Fig. 3(b) and the incoherent Sm $4f$ spectra in Fig. 2(c) at $T \simeq 80$ K. Intriguingly, g-SmS has a minimum volume at $T \simeq 80$ K [48], which signifies the close connection of a broad maximum in the resistivity with the mixed-valent nature of SmS. Hence we assign $T \simeq 80$ K as T_{VT} . Interestingly, SmB₆ also exhibits a similar broad maximum feature in the resistivity [49] and a minimum volume [50] near $T \simeq 150$ K. The resistivity increases below $T \simeq 40$ K, at which the coherent $4f_{5/2}$ -band starts to emerge in Fig. 2(c). The resistivity hump at $T \simeq 26$ K indicates that T_{coh} is around 26 K. In conventional metallic Kondo lattices, the resistivity decreases monotonically to zero below T_{coh} . The behavior near T_{coh} was explained in the two-fluid model by a crossover from the Kondo spin-liquid (KSL) to Kondo Fermi-liquid (KFL) [45]. We use a term of Kondo-liquid (KL) in Fig. 3(c) to comprise both KSL and KFL phases.

Thus g-SmS exhibits a crossover from mixed-valence to Kondo lattice behavior upon cooling [51, 52]. The charge-fluctuation that starts to be effective at $T \simeq 80$ K becomes almost frozen at $T \simeq 20$ K, as shown in

Fig. 3(b). Then, the spin-fluctuation becomes dominant near $T \simeq 25$ K, so as to activate the Kondo screening. In fact, the effective hybridization obtained in the DMFT becomes the largest near $T = 25$ K [39].

Meanwhile, $T \simeq 20$ K of the dip structure coincides with T , at which the upper $4f_{5/2}$ flat band (Δ_7 doublet) along $\Gamma - X$ is detached from E_F . Thus the resistivity up-turn occurs due to the apparent pseudo-gap (PG) feature, and so we assign $T = 20$ K as T_{PG} . Actually, this kind of hump and dip structure in the resistivity has been observed in several Ce compounds of Kondo-insulator type, such as CeNiSn and CeRhSb [53, 54]. The third resistivity drop at $T = 13$ K occurs due to the complete formation of the coherent $4f_{5/2}$ band over the whole Brillouin zone. Below $T = 13$ K, the imaginary part of self-energy almost vanishes [39], whereby the crossover from the KL to the Landau Fermi-liquid (LFL) takes place [45]. So we assign $T = 13$ K as T_{FL} . Therefore, SmS undergoes several crossover transitions upon cooling, from VF liquid (VFL), KL, PG to LFL, as shown in Fig. 3(c). The energy scales T_{VT} , T_{coh} , T_{PG} , and T_{FL} , which are identified for SmS, are considered to be universal to characterize Kondo/mixed-valent semimetallic systems.

Finally, it should be pointed out that the resistivity behavior in SmS is quite different from that in SmB₆ that is a candidate of topological Kondo insulators. g-SmS is not a Kondo insulator but close to a Kondo semimetal, so that the conventional metallic resistivity behavior is expected to be realized at very low T .

In conclusion, in g-SmS, the coherent Sm $4f$ bands are formed upon cooling to produce the hybridization-induced pseudogap feature near E_F , which is accompanied by a Lifshitz-like topological transition in the FS. g-SmS is found to be not a topological Kondo semimetal in view of that the in-gap surface states are not topological states but are typical spin-polarized Rashba states. From the analysis of T -dependent resistivity of g-SmS, we have identified characteristic multiple energy scales, which are expected to govern the physics of Kondo/mixed-valent semimetallic systems universally.

Helpful discussions with Junwon Kim, J. H. Shim, B. H. Kim, Ki-Seok Kim, J. -S. Kang, J. D. Denlinger, J. W. Allen, and K. Sun are greatly appreciated. This work was supported by the NRF (No. 2009-0079947 and No. 2011-0025237), POSTECH BK21Plus Physics Division and BSRI grant, and the KISTI supercomputing center (No. KSC-2013-C3-010).

* Electronic address: rkdc1234@postech.ac.kr

† Electronic address: bimin@postech.ac.kr

[1] G. R. Stewart, Rev. Mod. Phys. **56**, 755 (1984).

[2] P. Coleman, C. Pépin, Q. Si and R. Ramazashvili J. Phys.: Condens. Matter **13** R723 (2001).

- [3] P. Gegenwart, Q. Si and F. Steglich, *Nature Physics* **4**, 186 (2008).
- [4] M. Dzero, K. Sun, V. Galitski, and P. Coleman, *Phys. Rev. Lett.* **104**, 106408 (2010).
- [5] T. Takimoto, *J. Phys. Soc. Jpn.* **80**, 123710 (2011).
- [6] M. Dzero, K. Sun, P. Coleman, and V. Galitski, *Phys. Rev. B* **85**, 045130 (2012).
- [7] C.-J. Kang, J.-W. Kim, K. Kim, J.-S. Kang, J. D. Denlinger, B. I. Min, arXiv:1312.5898 (2013).
- [8] J. Kim, K. Kim, C.-J. Kang, S. Kim, H. C. Choi, J.-S. Kang, J. D. Denlinger, and B. I. Min, *Phys. Rev. B* **90**, 075131 (2014).
- [9] N. Xu *et al.*, *Phys. Rev. B* **88**, 121102(R) (2013).
- [10] M. Neupane *et al.*, *Nat. Commun.* **4**, 2991 (2013).
- [11] D. J. Kim, J. Xia, Z. Fisk, *Nat. Mater.* **13**, 466 (2014).
- [12] D. J. Kim, S. Thomas, T. Grant, J. Botimer, Z. Fisk, J. Xia, *Sci. Rep.* **3**, 3150 (2013).
- [13] J. D. Denlinger, J. W. Allen, J.-S. Kang, K. Sun, J.-W. Kim, J. H. Shim, B. I. Min, D.-J. Kim, Z. Fisk, arXiv:1312.6637 (2013).
- [14] C.-H. Min, P. Lutz, S. Fiedler, B. Y. Kang, B. K. Cho, H.-D. Kim, H. Bentmann, and F. Reinert, *Phys. Rev. Lett.* **112**, 226402 (2014).
- [15] Z. Li, J. Li, P. Blaha, and N. Kioussis, *Phys. Rev. B* **89**, 121117(R) (2014).
- [16] V. N. Antonov, B. N. Harmon, and A. N. Yaresko, *Phys. Rev. B* **66**, 165208 (2002).
- [17] A. Svane, V. Kanchana, G. Vaitheeswaran, G. Santi, W. M. Temmerman, Z. Szotek, P. Strange, and L. Petit, *Phys. Rev. B* **71**, 045119 (2005).
- [18] C. M. Varma, *Rev. Mod. Phys.* **48**, 219 (1976).
- [19] P. Villars and L. D. Calvert, *Pearson's Handbook of Crystallographic Data for Intermetallic Phases* (ASM International, Materials Park, 1991).
- [20] M. Campagna, E. Bucher, G. K. Wertheim, and L. D. Longinotti, *Phys. Rev. Lett.* **33**, 165 (1974).
- [21] A. Jayaraman, V. Narayanamuri, E. Bucher, and R. G. Maines, *Phys. Rev. Lett.* **25**, 1430 (1970).
- [22] P. P. Deen, D. Braithwaite, N. Kernavanois, L. Paolasini, S. Raymond, A. Barla, G. Lapertot, and J. P. Sanchez, *Phys. Rev. B* **71**, 245118 (2005).
- [23] T. Ito, A. Chainani, H. Kumigashira, T. Takahashi, and N. K. Sato, *Phys. Rev. B* **65**, 155202 (2002).
- [24] T. Mizuno, T. Iizuka, S. Kimura, K. Matsubayashi, K. Imura, H. S. Suzuki, and N. K. Sato, *J. Phys. Soc. Jpn.* **77**, 113704 (2008).
- [25] M. B. Maple and D. Wohleben, *Phys. Rev. Lett.* **27**, 511 (1971).
- [26] J. M. D. Coey, S. K. Ghatak, M. Avignon, and F. Holtzberg, *Phys. Rev. B* **14**, 3744 (1976).
- [27] K. Matsubayashi, K. Imura, H. S. Suzuki, G. Chen, N. Mori, T. Nishioka, K. Deguchi, and N. K. Sato, *J. Phys. Soc. Jpn.* **76**, 033602 (2007).
- [28] P. Wachter, *Handbook of the Physics and Chemistry of Rare Earths*, edited by K. A. Gschneidner, L. Eyring, and S. Hüfner (North-Holland, Amsterdam, 1994), Vol. 19, p. 177.
- [29] J. Flouquet, Y. Haga, P. Haen, D. Braithwaite, G. Knebel, S. Raymond, S. Kambe, *J. Magn. Magn. Mater.* **272-276**, 27 (2004).
- [30] R. M. Martin and J. W. Allen, *J. Appl. Phys.* **50**, 7561 (1979).
- [31] S. M. Shapiro, R. J. Birgeneau, and E. Bucher, *Phys. Rev. Lett.* **34**, 470 (1975).
- [32] A. Barla *et al.*, *Phys. Rev. Lett.* **92**, 066401 (2004).
- [33] K. Imura, K. Matsubayashi, H. S. Suzuki, N. Kabeya, K. Deguchi, and N. K. Sato, *J. Phys. Soc. Jpn.* **78**, 104602 (2009).
- [34] F. Lapiere, M. Ribault, F. Holtzberg, and J. Flouquet, *Solid State Commun.* **40**, 347 (1981).
- [35] M. Konczykowski, J. Morillo, and J. P. Senateur, *Solid State Commun.* **40**, 517 (1981).
- [36] M. Konczykowski, F. Lapiere, P. Haen *J. Magn. Magn. Mater.* **47-48**, 274 (1985).
- [37] K. Imura, K. Matsubayashi, H. S. Suzuki, K. Deguchi, N. K. Sato, *Physica B* **404**, 3028 (2009).
- [38] P. Blaha, K. Schwarz, G. K. H. Madsen, D. Kvasnicka, and J. Luitz, Wien2k (Karlheinz Schwarz, Technische Universität Wien, Austria, 2001).
- [39] See the Supplemental Materials for the DFT, DFT+*U*, and DMFT results for b-SmS and g-SmS, and *T*-dependent DMFT physical parameters.
- [40] G. Kotliar, S. Y. Savrasov, K. Haule, V. S. Oudovenko, O. Parcollet, and C. A. Marianetti, *Rev. Mod. Phys.* **78**, 865 (2006).
- [41] K. Haule, C.-H. Yee, and K. Kim, *Phys. Rev. B* **81**, 195107 (2010).
- [42] For the model slab calculation, the Wannier downfolding scheme was employed to fit the bulk band structure obtained by the DFT+10×*f*-SOC (see the supplement). We have also performed the DFT slab calculation and confirmed that results from the model and DFT slab calculations are essentially the same.
- [43] P. Wachter, A. Jung, and P. Steiner, *Phys. Rev. B* **51**, 5542(R) (1995).
- [44] H. C. Choi, B. I. Min, J. H. Shim, K. Haule, and G. Kotliar, *Phys. Rev. Lett.* **108**, 016402 (2012).
- [45] S. Nakatsuji, D. Pines, and Z. Fisk, *Phys. Rev. Lett.* **92**, 016401 (2004); Y.-f. Yang and D. Pines, *Phys. Rev. Lett.* **100**, 096404 (2008); Y.-f. Yang and D. Pines, *Proc. Natl. Acad. Sci.* **109**, E3060 (2012).
- [46] I. M. Lifshitz, *Sov. Phys. JETP* **11**, 1130 (1960).
- [47] M. Mizumaki, S. Tsutsui, and F. Iga, *J. Phys. Conf. Ser.* **176**, 012034 (2009).
- [48] K. Iwasa, T. Tokuyama, M. Kohgi, N. K. Sato, N. Mori, *Physica B* **359-361**, 148 (2005).
- [49] A. Kebede *et al.*, *Physica B* **223-224**, 256 (1996).
- [50] V. A. Trounov *et al.*, *J. Phys.: Condens. Matter* **5**, 2479 (1993).
- [51] P. Coleman, *Handbook of Magnetism and Advanced Magnetic Materials*, Edited by Helmut Kronmüller and Stuart Parkin. Vol 1: Fundamentals and Theory. John Wiley and Sons, 95-148 (2007).
- [52] P. Kumar and N. S. Vidhyadhiraja, *J. Phys.: Condens. Matter* **23**, 485601 (2011).
- [53] T. Takabatake *et al.*, *Phys. Rev. B* **41**, 9607(R) (1990).
- [54] S. K. Malik and D. T. Adroja, *Phys. Rev. B* **43**, 6277(R) (1991).

Supplemental Material:
**Topological properties and the dynamical crossover from mixed-valence
to Kondo-lattice behavior in golden phase of SmS**

A BLACK PHASE OF SMS (B-SMS)

DFT band structure

For the DFT calculations, we have employed the all-electron FLAPW band method implemented in Wien2k [1]. We used $17 \times 17 \times 17$ k -point mesh in the full Brillouin zone. The muffin-tin radii R_{MT} were set to 2.50 and 2.30 a.u. for Sm and S, respectively, and the product of R_{MT} and the maximum reciprocal lattice vector K_{max} was chosen as $R_{MT} \cdot K_{max} = 8$. We used the maximum L value of 10 for the waves inside the atomic spheres and the largest reciprocal lattice vector G_{max} of 12 in the charge Fourier expansion.

Figure S1 shows the band structures and densities of states (DOSs) of a black phase of SmS (b-SmS) obtained by the DFT schemes. Figure S1(a) shows symmetry decomposed band structure of b-SmS in the GGA + SOC scheme (SOC: spin-orbit coupling). Since Sm $4f$ -electrons feel much larger SOC than the cubic crystal field, the SOC bases incorporating the cubic crystal field should be utilized [2, 3]. The cubic crystal field splits $4f_{5/2}$ states at Γ into lower Γ_7 doublet and higher Γ_8 quartet, as in SmB₆ [3]. Sm $4f$ bands are dominant near the Fermi level (E_F), and $4f_{5/2}$ and $4f_{7/2}$ states are located mainly below and above E_F , respectively. The splitting between $4f_{5/2}$ and $4f_{7/2}$ states is about 0.75 eV, which is related to the strength of the SOC of $4f$ electrons in Sm ion. In fact, most of $4f_{7/2}$ states are to be shifted up in energy due to the strong correlation effect of $4f$ -electrons.

Sm $5d$ t_{2g} characters are also shown in order to visualize the hybridization between the Γ_7 doublet and t_{2g} band. Since the lobes of e_g and t_{2g} orbitals of Sm $5d$ electrons are along and away from the anion sulfur ions, respectively, the energy of t_{2g} band is to be lower than that of e_g band. This feature in SmS is contrary to that in SmB₆, for which the e_g band is lower in energy than the t_{2g} band because the lobes of t_{2g} orbitals are toward anion boron ions [3]. Therefore, in SmB₆, the f - d hybridization occurs between the Γ_7 doublet and e_g band, while, in SmS, it occurs between the Γ_7 doublet and t_{2g} band. At X , the t_{2g} band is located below $4f_{5/2}$ bands, and so the order of parities is changed. The valence state of Sm in the GGA + SOC scheme is estimated to be 2.56+, which is far from the semiconducting black phase of the valence state of Sm, 2+. Furthermore, the band gap is not obtained which is contrary to the experiment.

Figure S1(b) presents the symmetry-projected partial DOSs (PDOSs) of b-SmS in the GGA + SOC scheme. Sm $4f_{5/2}$ DOS is projected into the relativistic double group bases and Sm $4f_{7/2}$ and $5d$ t_{2g} PDOSs are also provided. It is seen that the DOS at E_F is not zero, implying that the system is not an insulator. Rather it is semimetallic, as shown in Fig. S1(a).

Figure S1(c) and (d) show electronic structures of b-SmS in the GGA + SOC + U scheme (U : Coulomb correlation of Sm $4f$ electrons). When $U_{eff} = 7.6$ eV, it gives an insulating phase with the band gap of 87 meV, which is quite comparable to the experimental band gap of ~ 0.15 eV [4]. Once the semiconducting phase of SmS is obtained, the parity inversion does not happen, which results in the trivial \mathbb{Z}_2 topological number. The valence state of Sm is estimated to be 2.23+, which is close to 2+. However, the band symmetries at high symmetry k -points are different from those in the GGA + SOC scheme, which turns out to be wrong in view of the DMFT results (see Fig. 2(c) in the main text).

Figure S1 (e) and (f) show symmetry decomposed band structure and PDOS of b-SmS in the GGA + SOC with 10 times enhanced SOC of Sm $4f$ -electron (10 $\times f$ -SOC scheme). Due to the artificially large SOC strength, the $4f_{7/2}$ bands are shifted up to the higher energy side. In contrast to the GGA + SOC + U scheme, the band symmetries at high symmetry k -point in the 10 $\times f$ -SOC scheme are consistent with those of the GGA + SOC scheme. Sm $5d$ t_{2g} band hybridizes with Γ_7 doublet, resulting in the hybridization gap near X . The valence state of Sm is estimated to be 2.27+.

Thus the DFT schemes can not describe the ground state electronic structure of b-SmS properly. Also, according to the angle-resolved photoemission spectroscopy (ARPES) experiment [5], Sm $4f$ bands are very flat and distributed broadly from 1 to 4 eV below E_F , which is different from the DFT results. This is due to the strong correlation effect in $4f$ electrons, which cannot be captured in conventional DFT calculations.

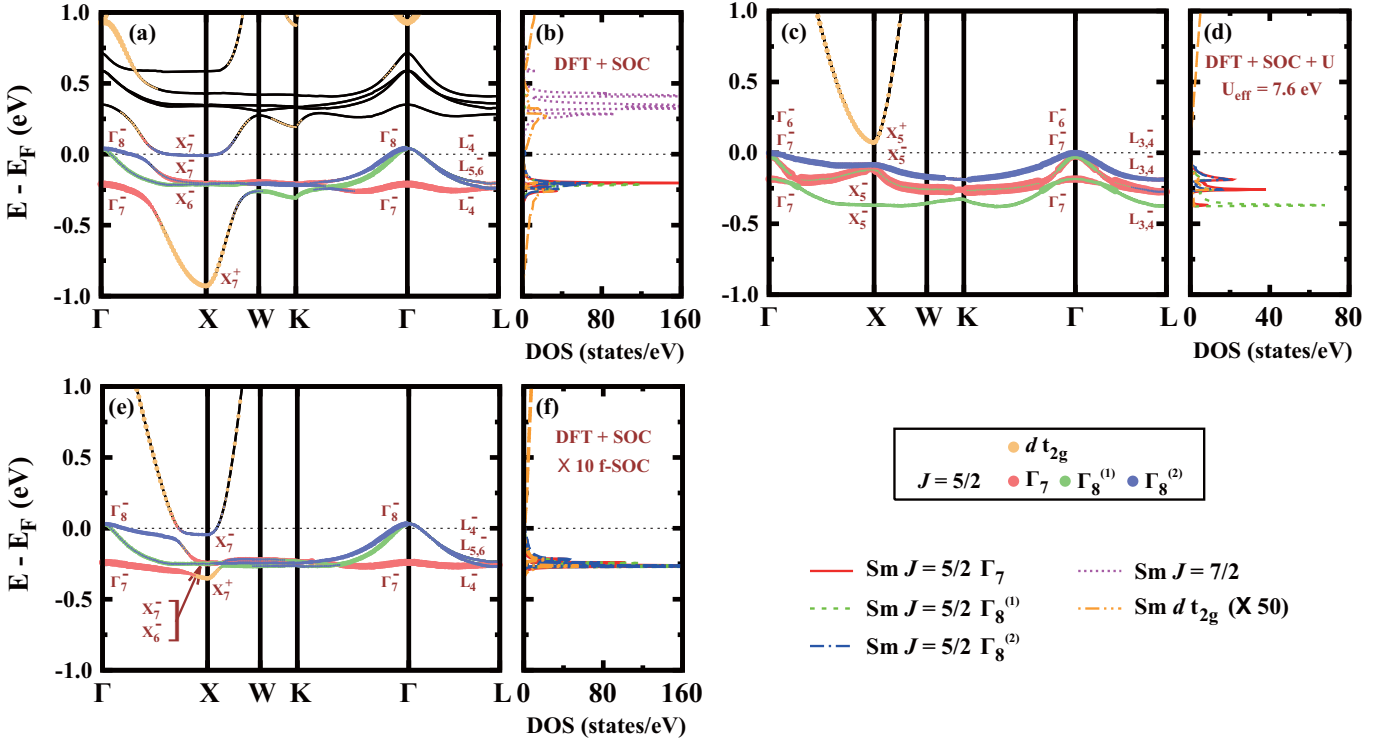


FIG. S1: (Color Online) Band structures and DOSs of a black phase of SmS ($a = 5.953 \text{ \AA}$) in the DFT schemes. (a) Symmetry decomposed band structure with the relativistic double group bases in the GGA + SOC scheme, which gives erroneously the slightly overlapped semimetallic state. Sm $5d t_{2g}$ band is seen to be hybridized with Γ_7 doublet bands. The valence state of Sm is obtained to be 2.56+ in this case. (b) Symmetry projected partial DOS (PDOS) in the GGA + SOC scheme. Sm $J = 5/2$ DOS are projected into the double group bases. Sm $5d t_{2g}$ DOS is magnified 50 times for a clear view. (c) and (d) present symmetry decomposed band structure and PDOS in the GGA + SOC + U ($U_{eff} = 7.6 \text{ eV}$) scheme, which seems to describe correctly a semiconducting b-SmS with the band gap of 87 meV. The valence state of Sm is obtained to be 2.23+. However, band symmetries at high symmetry k -points in this scheme are different from those in the GGA + SOC scheme. (e) and (f) show symmetry decomposed band structure and PDOS in the GGA + SOC with 10 times enhanced SOC of Sm $4f$ -electron ($10 \times f$ -SOC scheme). Due to the large SOC strength, the $J = 7/2$ band is shifted up to a higher energy side. In contrast to the GGA + SOC + U scheme, band symmetries at high symmetry k -points in this scheme preserve those of the GGA + SOC scheme. Sm t_{2g} band hybridizes with Γ_7 doublet, resulting in the hybridization gap near X. The valence state of Sm is obtained to be 2.27+.

DMFT band structure

Figure S2 shows the band structure and DOS of b-SmS ($a = 5.9 \text{ \AA}$) obtained by the charge self-consistent DFT + DMFT scheme at $T = 11.6 \text{ K}$. It is seen that the insulating electronic structure is correctly described by the DMFT scheme. The obtained band gap and the valence configuration of Sm are 0.46 eV and 2.06+, respectively. The band structure in Fig. S2 is very similar to that obtained by the periodic Anderson model calculation [6], and consistent with ARPES data [5]. The partial DOS in Fig. S2b shows $4f$ multiplets, which are in good agreement with XPS data [7]. Since the Sm d -band is above the Sm f -band, b-SmS is a topologically trivial insulator.

A GOLDEN PHASE OF SMS (G-SMS)

Band structure in the DFT + SOC with $10 \times f$ -SOC scheme

Figure S3 provides electronic structures of g-SmS ($a = 5.6 \text{ \AA}$) in the GGA + SOC with $10 \times f$ -SOC scheme. The electronic structures in Fig. S3 are quite similar to those of g-SmS described by the DMFT at low T (see Fig. 2(c) in the main text). But, the number of f -electron (n_f) in the DFT + SOC with $10 \times f$ -SOC scheme is 5.64 ($\text{Sm}^{2.36+}$), while n_f in the DMFT scheme is 5.27 ($\text{Sm}^{2.73+}$).

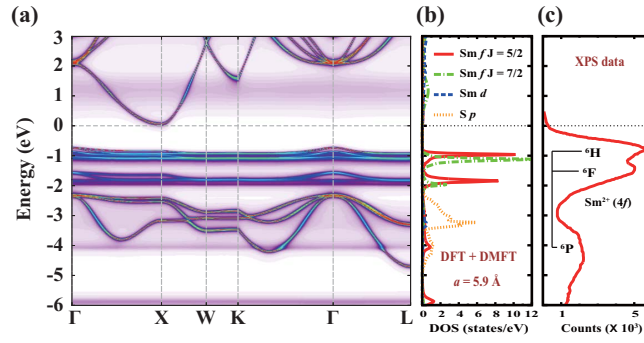


FIG. S2: (Color Online) Electronic structure of b-SmS. (a) The DMFT band structure of insulating b-SmS ($a = 5.9 \text{ \AA}$) at $T = 11.6 \text{ K}$. On-site Coulomb and exchange energies of $U = 6.1 \text{ eV}$ and $J = 0.8355 \text{ eV}$ were adopted. (b) Partial DOS of b-SmS. (c) XPS data for b-SmS taken from Ref. [7].

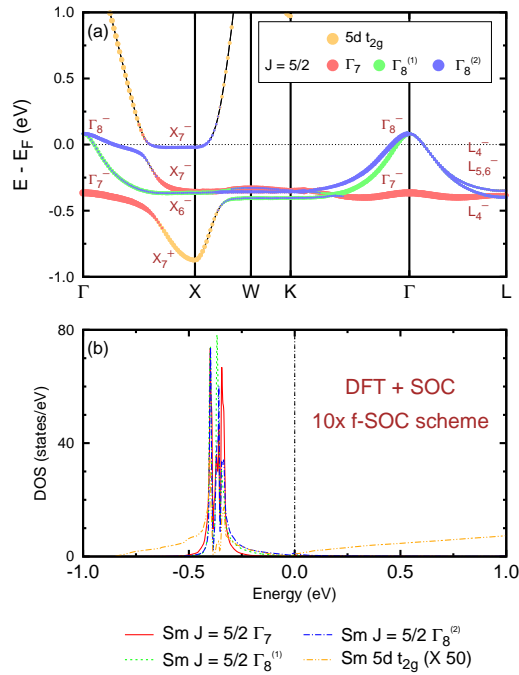


FIG. S3: (Color Online) Band structure and PDOS of golden phase of SmS (g-SmS) ($a = 5.6 \text{ \AA}$) in the GGA + SOC with $10 \times f$ -SOC scheme. (a) Symmetry decomposed band structure with the relativistic double group bases. Sm $5d t_{2g}$ band is seen to be hybridized with Γ_7 doublet bands. The valence state of Sm is obtained to be $2.36+$ in this case. (b) Symmetry projected PDOS. Sm $J = 5/2$ DOS is projected into the double group bases. Sm $5d t_{2g}$ DOS is magnified 50 times for a clear view.

Temperature-dependent DMFT physical parameters

Figure S4 presents the temperature (T)-dependent physical properties of g-SmS ($a = 5.6 \text{ \AA}$) described by the DMFT. Figure S4(a) and (b) show the renormalization factor Z and effective mass m^* versus T . Upon cooling, Z of $J = 5/2$ ($J = 7/2$) increases (decreases), resulting in decreasing (increasing) m^* of $J = 5/2$ ($J = 7/2$). Relaxation times of both $J = 5/2$ and $J = 7/2$ diverge upon cooling, as shown in Fig. S4(c), suggesting the crossover to the Landau Fermi liquid behavior at low T .

Figure S4(d) provides the T -dependent behavior of the hybridization function at E_F ($\Delta(E_F)$), which is closely

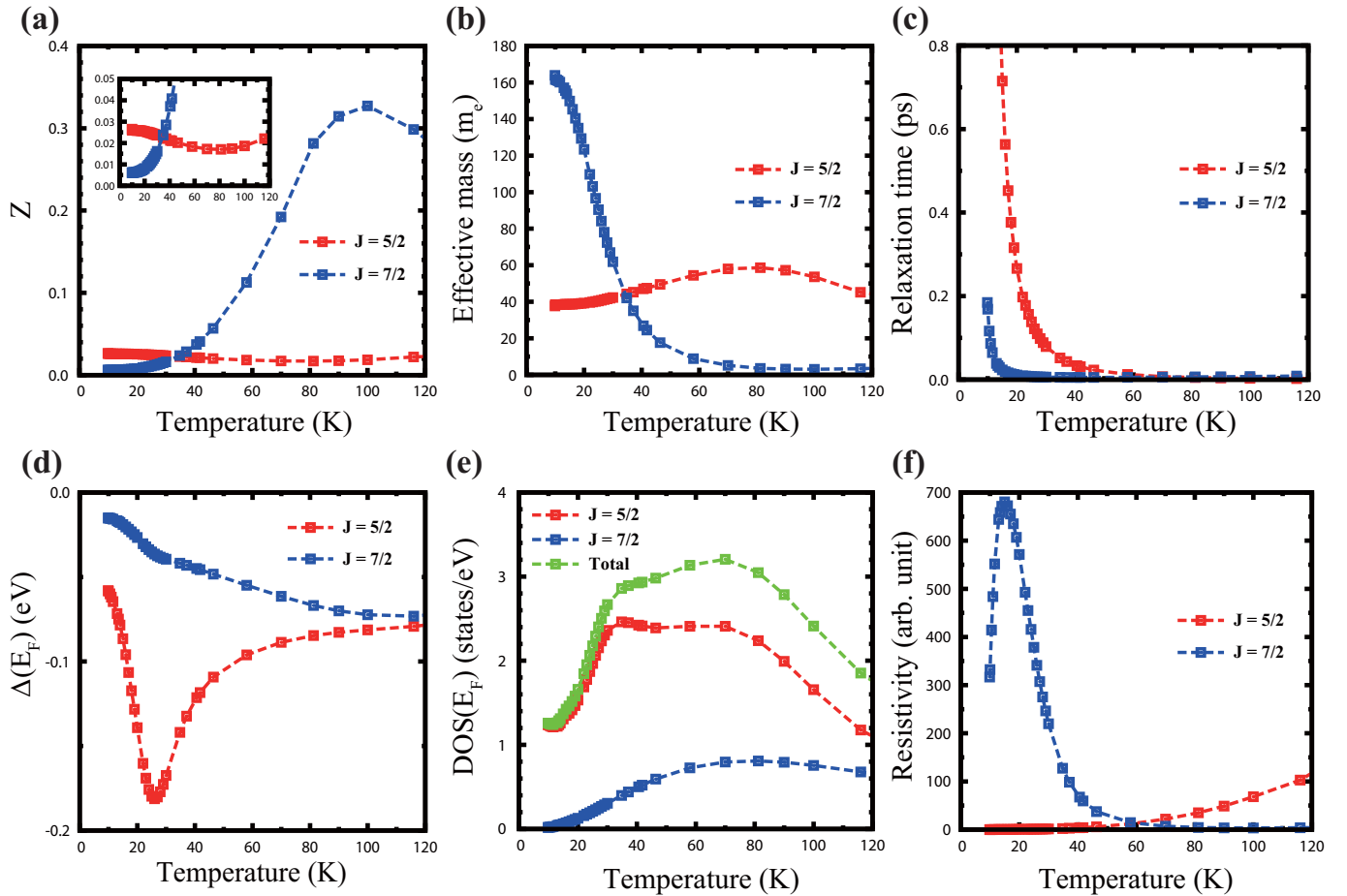


FIG. S4: (Color Online) T -dependent DMFT physical parameters in g-SmS ($a = 5.6 \text{ \AA}$). (a) and (b) represent the renormalization factor Z and effective mass m^* versus T . Upon cooling, Z of $J = 5/2$ increases, while that of $J = 7/2$ decreases. (Inset shows this trend clearly.) The behavior of m^* is just opposite, because $m^* = 1/Z$. (c) Relaxation time versus T . Both relaxation times of $J = 5/2$ and $J = 7/2$ diverge at low T , suggesting the crossover to the Landau Fermi liquid behavior. (d) T -dependent behavior of the hybridization function at E_F ($\Delta(E_F)$). It has the largest value near $T = 25 \text{ K}$ to produce the strong Kondo screening behavior. (e) DOS at E_F versus T . The total DOS at E_F increases first and then decreases below $T \simeq 70 \text{ K}$. (f) Resistivity versus T obtained by the Drude model. The resistivity drop for $J = 7/2$ is clearly shown at $T \simeq 13 \text{ K}$, which is also captured in the DMFT result (see Fig. 3(c) in the main text).

related to the Kondo interaction strength. Hence the largest $\Delta(E_F)$ value near $T \simeq 25 \text{ K}$ suggests that Kondo screening behavior becomes strongly enhanced at this temperature range. On the other hand, the total DOS at E_F in Fig. S4(e) increases first and then decreases below $T \simeq 70 \text{ K}$. Note that the total DOS at E_F is saturated at low- T , indicating the full lattice coherence below $T \simeq 13 \text{ K}$.

Fig. S4(f) shows the resistivity versus T obtained by the Drude model. The resistivity drop for $J = 7/2$ is clearly shown below $T \simeq 13 \text{ K}$, which is also captured in the DMFT result (see Fig. 3(c) in the main text). It implies that the crossover from the Kondo liquid to the Landau Fermi liquid occurs below $T \simeq 13 \text{ K}$.

The images for moving pictures containing T -dependent band structures and Fermi surfaces (T-band-movie1 and T-FS-movie2) are provided for the additional Supplementary Information.

* Electronic address: rkdc1234@postech.ac.kr

† Electronic address: bimin@postech.ac.kr

- [1] P. Blaha, K. Schwarz, G. K. H. Madsen, D. Kvasnicka, and J. Luitz, Wien2k (Karlheinz Schwarz, Technische Universität Wien, Austria, 2001).
- [2] R. Pappalardo, J. Chem. Phys. **34**, 1380 (1961).

- [3] C.-J. Kang, J.-W. Kim, K. Kim, J.-S. Kang, J. D. Denlinger, B. I. Min, arXiv:1312.5898 (2013).
- [4] C. M. Varma, Rev. Mod. Phys. **48**, 219 (1976).
- [5] T. Ito, A. Chainani, H. Kumigashira, T. Takahashi, and N. K. Sato, Phys. Rev. B **65**, 155202 (2002).
- [6] C. Lehner, M. Richter, and H. Eschrig, Phys. Rev. B **58**, 6807 (1998).
- [7] M. Campagna, E. Bucher, G. K. Wertheim, and L. D. Longinotti, Phys. Rev. Lett. **33**, 165 (1974).